ACS APPLIED MATERIALS & INTERFACES

www.acsami.org

Research Article

Synergistically Chemical and Thermal Coupling between Graphene Oxide and Graphene Fluoride for Enhancing Aluminum Combustion

Yue Jiang,[#] Sili Deng,[#] Sungwook Hong,[#] Subodh Tiwari, Haihan Chen, Ken-ichi Nomura, Rajiv K. Kalia, Aiichiro Nakano, Priya Vashishta, Michael R. Zachariah, and Xiaolin Zheng*

Cite This: *ACS Appl. Mater. Interfaces* 2020, 12, 7451−7458

Read Online

ACCESS | Metrics & More | Article Recommendations | Supporting Information

ABSTRACT: Metal combustion reaction is highly exothermic and is used in energetic applications, such as propulsion, pyrotechnics, powering micro- and nano-devices, and nanomaterials synthesis. Aluminum (Al) is attracting great interest in those applications because of its high energy density, earth abundance, and low toxicity. Nevertheless, Al combustion is hard to initiate and progresses slowly and incompletely. On the other hand, ultrathin carbon nanomaterials, such as graphene, graphene oxide (GO), and graphene fluoride (GF), can also undergo exothermic reactions. Herein, we demonstrate that the mixture of GO and GF significantly improves the performance of Al combustion as interactions between GO and GF provide heat and radicals to accelerate Al oxidation. Our experiments and reactive molecular dynamics simulation reveal that GO and GF have strong chemical and thermal couplings through radical reactions and heat released from their oxidation reactions. GO facilitates the dissociation of GF, and GF accelerates the disproportionation and oxidation of GO. When the mixture of GO and GF is added to micron-sized Al particles, their synergistic couplings generate reactive oxidative species, such as CF_x and CF_xO_y, and heat, which greatly accelerates Al combustion. This work demonstrates a new area of using synergistic couplings between ultrathin carbon nanomaterials to accelerate metal combustion and potentially oxidation reactions of other materials.

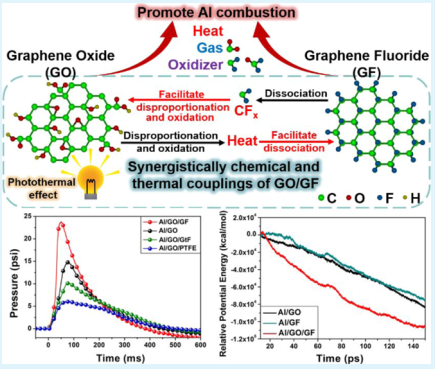

KEYWORDS: *energetic materials, graphene oxide, graphene fluoride, flash ignition, aluminum combustion*

1. INTRODUCTION

Combustion of metal-based energetic materials is an exothermic process that generates heat, light, and thrust rapidly, and it is of great interest for a variety of applications ranging from aerospace to nanoscale, including propulsion, pyrotechnics, micro- and nano-devices in microelectromechanical systems, and synthesis of nanomaterials.[1−5] Aluminum (Al) is the most popular metal for those applications due to its earth abundance, low toxicity, and high specific energy density.[6] In those applications, Al is typically used in the forms of nano- or micron-sized particles. Nano-sized Al (n-Al) has a lower ignition temperature and higher reactivity than the micron-sized Al (μ-Al),[7,8] but n-Al tends to agglomerate and has a larger fraction of inert Al_2O_3. For example, a 50 nm diameter n-Al particle has about a 2 nm thick Al_2O_3 shell, occupying 30% of the total n-Al mass. Hence, μ-Al particles are still commonly used in practical applications.[9,10] It is highly desirable to improve the combustion performance of μ-Al particles to be similar to n-Al for the aforementioned applications.

Recently, we have demonstrated that ultrathin graphene oxide (GO) lowers the ignition energy and increases the energy release rate of μ-Al particles with a Xe lamp flash ignition.[11] The enhancement effect of GO is attributed to its exothermic disproportionation and oxidation reactions, catalytic effects,[11−14] and excellent light absorption properties.[15−17] In addition, we showed that the μ-Al/GO composites exhibit much better combustion performance than the μ-Al/metal oxides (e.g., WO_3) thermite mixtures with the same weight percentage of μ-Al. Nevertheless, the addition of GO inevitably lowers the specific energy density of μ-Al particles. It is desirable to increase the energy density of Al/GO while maintaining or even improving its combustion performance.

Fluorination of Al is known to have a much higher heat of reaction than that of Al oxidation (55.7 kJ/g vs 35.6 kJ/g).[18] Moreover, fluorine reacts with the native Al_2O_3 layer to form more volatile AlF_3, which enhances both the ignition and the combustion of Al.[19,20] Hence, a potential solution for increasing the energy density of Al/GO is to replace some GO with fluorine-containing oxidizers. In fact, fluoropolymers, such as polytetrafluoroethylene (PTFE) and polyvinylidene fluoride, have been used as oxidizers and/or binders in Al-

Received: November 10, 2019
Accepted: January 17, 2020
Published: January 17, 2020

https://dx.doi.org/10.1021/acsami.9b20397
ACS Appl. Mater. Interfaces 2020, 12, 7451−7458

based energetic composites or as surface-coating materials on Al particles to enhance their energetic performance.[21−25] In addition, graphite fluoride (GtF) was shown to enhance the combustion of Al and Mg particles.[26,27]

Here, we investigate a new type of fluorine-containing oxidizer, exfoliated monolayer graphene fluoride (GF),[28,29] and combine GF with GO to enhance the combustion performance of μ-Al particles. GF is fully fluorinated graphene, and each carbon atom in the basal plane of GF is sp^3 hybridized and bonded with one fluorine atom.[30,31] GF has a number of properties suitable for enhancing Al combustion. First, GF contains ~50 at. % of fluorine, which is comparable to that of PTFE (66.6 at. %) and GtF (~50 at. %), but all those fluorine atoms in GF are exposed on the surface and easily accessible for reacting with Al. Secondly, GF, similar to GO, has a low density of ~2.7 g/cm^3,[32,33] so it helps to keep the specific energy density of the composite high. Finally, GF can be considered energetic as it decomposes and reacts with oxygen in the air at ~ 400−600 °C, generating CF_x and CF_xO_y species that can further react with Al.[34,35]

In this study, we experimentally and computationally compared the combustion performance of three mixtures: μ-Al/GO, μ-Al/GF, and μ-Al/GO/GF. Motivated by our previous study on the enhanced optical ignition of μ-Al by the intrinsic chemical activity of GO,[11] our current study used the chemical and/or thermal coupling effect of GO and GF to enhance the ignition and combustion of μ-Al and further revealed the underlying mechanism responsible for the coupling effect of GO/GF. We found that the combination of GO and GF provides synergistic enhancements for μ-Al ignition and combustion through both Xe flash ignition experiments and reactive molecular dynamics (RMD) simulation. The enhancement mechanism is schematically explained in Figure 1. GO is rapidly heated by the Xe flash

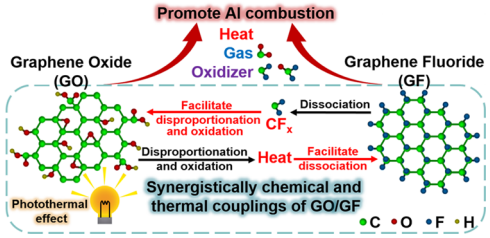

Figure 1. Proposed mechanism for GO/GF chemical and thermal couplings. Schematics of the synergistically thermal and chemical coupling between GF and GO and its effects for enhancing the energetic performance of Al (green, C atoms; red, O atoms; blue, F atoms; yellow, H atoms).

lamp through the photothermal effect,[36−38] which triggers its exothermic disproportionation and oxidation reactions. Those reactions release heat and oxygenated species to initiate the dissociation of GF, which generates CF_x species to further react with GO, releasing more heat and radicals. The interaction between GO and GF produces heat and oxidative radicals that facilitate Al combustion. In addition, we found that GO/GF is more effective than GO/PTFE and GO/GtF in enhancing μ-Al combustion. These results suggest that the mixture of GO/GF is an effective energetic additive to synergistically promote μ-Al combustion. Finally, to our best knowledge, this is the first study demonstrating the chemical and/or thermal couplings between GF and GO.

2. METHODS

2.1. Material Preparation. Al/GO/GF (80/10/10 wt %) composites were prepared by a mechanical mixing method. We first sonicated 10 mg of GO powder synthesized by the Hammer's method (0.5−5 μm in diameter, 0.8−1.2 nm in thickness, XFNANO), and 10 mg of GF powder prepared by high-temperature fluorination of graphene by F_2 (0.4−5 μm in diameter, 0.8 nm in thickness, XFNANO) in ethanol (1 mg/mL) for 2 h, separately. Then, the suspensions of GO and GF were mixed together, and the mixture was sonicated for another 1 h. Meanwhile, 80 mg of Al particles (3.0−4.5 μm in diameter, Alfa Aesar) were dispersed in 8 mL of ethanol by sonication for 30 min. After that, the GO/GF suspension was added to the Al suspension and sonicated for 1 h. The mixture powders were collected by filtration and fully dried on a hotplate at 60 °C for 1 h and subsequently in a vacuum desiccator for 12 h. We used the same method to prepare other samples of GO/GF (50/50 wt %), Al/GO (80/20 wt %), Al/GF (80/20 wt %), Al/GO/GtF (80/10/10 wt %), and Al/GO/PTFE (80/10/10 wt %). The GtF powders are 4−10 μm in diameter and 5−10 nm in thickness (XFNANO), and the PTFE powders are 100−200 nm in diameter (DuPont).

2.2. Thermal Analysis of Samples with Thermogravimetry Analysis/Differential Scanning Calorimetry. To investigate the thermal behaviors of GO and GF, the evolution of mass and heat flow of GO, GF, and GO/GF mixture heated in the air was investigated by the combination of thermogravimetry analysis and differential scanning calorimetry (TGA/DSC, Setaram LABSYS Evo). In each test, an alumina crucible of 100 μL with 4 mg of the sample inside was heated at a rate of 10 °C/min from 100 to 800 °C in the air (40 sccm). The baseline correction of the sample TGA and DSC curves was performed by subtracting the TGA and DSC curves of the empty alumina crucible with the same heating process. The heat release of each exothermic peak was obtained by integrating the peak area (illustrated as first ΔH and second ΔH in Figure 2b) of each DSC

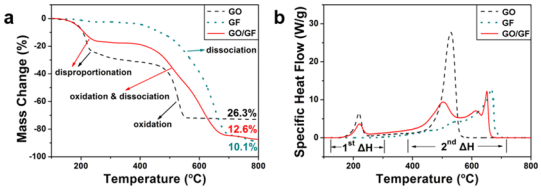

c

Sample	1st ΔH (kJ/g)	2nd ΔH (kJ/g)
GO	1.36	8.58
GF	-	7.50
GO/GF	1.15	9.36

d

Sample	Species	T_{onset}/°C
GO	C_xO_y	373 ± 50
GF	CF_x & C_xO_y	717 ± 50
GO/GF	C_xO_y	362 ± 50
GO/GF	CF_x	622 ± 50

Figure 2. Thermal analysis of GO, GF, and GO/GF mixture showing the thermal and chemical couplings between GO and GF. (a) TGA and (b) DSC results of GO, GF, and GO/GF being heated from 100 to 800 °C at 10 °C/min in the air (the numbers labeled in (a) are the mass percentages of the residual materials after experiments); (c) specific heat release calculated by integrating the exothermic peaks labeled in (b) DSC curves of GO, GF, and GO/GF samples; (d) onset temperatures for the release of carbon oxide species C_xO_y (including CO_2, CO, C, and O) and carbon fluorides species (CF_x), measured by T-jump TOFMS experiments, which resistively heated the sample coated on a Pt filament to ~1000 °C in 3 ms at 2.0 × 10^{-6} Torr.

curve. Similar TGA/DSC experiments were also conducted by heating 5 mg of Al/GO (80/20 wt %) and Al/GO/GF (80/10/10 wt %) samples from 100 to 1250 °C to investigate their thermal behaviors.

2.3. Temperature-Jump (T-Jump) Experiments. GO, GF, and GO/GF mixture (50/50 wt %) were analyzed with a T-jump electron ionization mass spectrometer.[39] The electron energy was set at 70 eV. The sample was first dispersed in ethanol and sonicated for 1 h. It was then coated onto a Pt filament 76 μm in diameter, which was resistively heated to ~1000 °C in 3 ms at about 2.0 × 10^{-6} Torr near

https://dx.doi.org/10.1021/acsami.9b20397
ACS Appl. Mater. Interfaces 2020, 12, 7451−7458

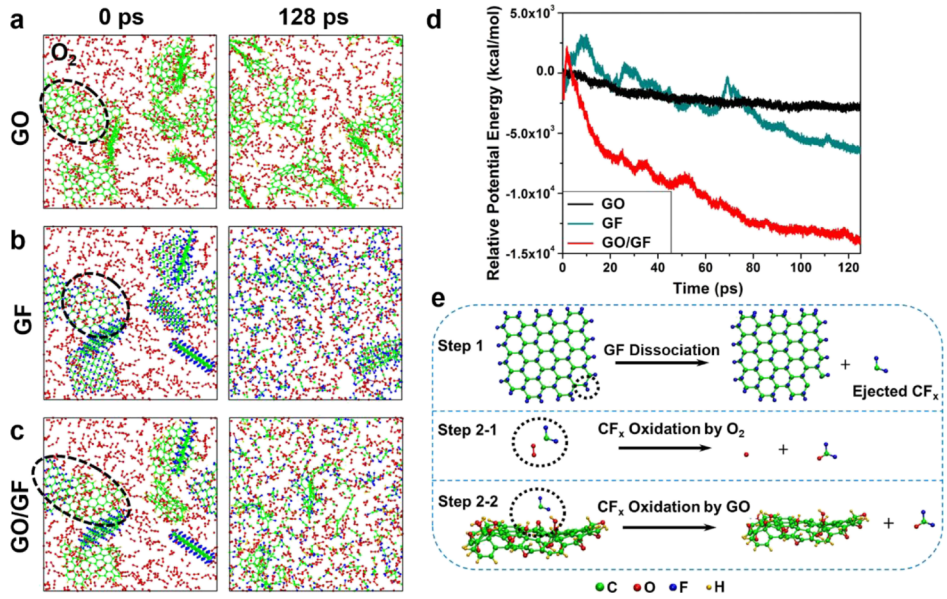

Figure 3. RMD simulation results reveal molecular-level thermal oxidation behaviors of GO, GF, and GO/GF mixture. Snapshots of RMD simulations for the thermal oxidation behavior of (a) GO, (b) GF, and (c) GO/GF 1:1 mixture with O_2 at 2000 K at 0 and 128 ps; (d) the relative potential energy vs time for the three different systems. A lower relative potential energy indicates more heat release; (e) reaction mechanisms for the oxidation of CF_x species by O_2 molecule or GO, derived by RMD simulations (green, C atoms; red, O atoms; blue, F atoms; yellow, H atoms).

the ionization region of the mass spectrometer. The time-of-flight measurement was triggered by the T-jump heating pulse to measure the gas species released/generated from heating the filament. The temporal voltage and current of the T-jump probe were recorded during heating, allowing resistivity to be obtained and related to instantaneous temperature and mapped against mass spectra.

2.4. RMD Simulation of Systems with and without Al. We used the ReaxFF[40,41] reactive force field to investigate the chemical reactions of GO, GF, and Al with GO and GF. Because the entire system contains three different types of materials, multiple ReaxFF parameters were merged into a single force field (i.e., Al/C/H/O, C/H/F, and F−O interactions employed by Hong and van Duin,[42] Rahnamoun and van Duin,[43] and Kim et al.,[44] respectively). For RMD simulations, we modeled a pre-oxidized Al slab (5126 atoms), a single GO sheet (134 atoms), and a single GF sheet (136 atoms). We used an orthogonal simulation cell of 48.54 Å × 49.47 Å × 155.0 Å that contains the pre-oxidized Al slab model at the bottom, 16 GO/16 GF sheets (or 16 GO/16 GF sheets without Al), and 2000 randomly distributed O_2 molecules. We applied a wall boundary condition in the *z*-direction of the simulation domain to prevent reactions between the bottom of the Al slab and gas species. The *NVT* ensemble (i.e., a constant number of atoms, a constant volume, and a constant temperature) with the Nosé−Hoover thermostat[45,46] was applied to the entire system. The detailed conditions of our RMD simulation can be found in our previous work.[11]

3. RESULTS AND DISCUSSION

3.1. Experimental Comparison of Reaction Characteristics of GO, GF, and GO/GF Mixture in Air. We first experimentally compare the reactive and thermal release properties of GO, GF, and GO/GF mixtures in the air in the absence of Al. Those properties were determined under both a slow heating rate (10 °C/min) using TGA and DSC and under a high heating rate (>10^5 °C/s) using the T-jump electron ionization mass spectrometer.[39] The TGA/DSC results are shown in Figure 2a−c, and the T-jump results are shown in Figure 2d. Under the slow heating condition, as shown in Figure 2a−c, pure GO first undergoes disproportionation reaction at 200 °C and is further oxidized at 500 °C.[11,13] In comparison, pure GF starts to dissociate at 420 °C.[34,47] For the mixture of GO and GF with the 1:1 mass ratio, its first exothermic peak (first ΔH in Figure 2b) starts around 200 °C, similar to GO, and the second exotherm (second ΔH in Figure 2b) starts at ∼400 °C, which is earlier than both the second exothermic (oxidation) peak of GO and the dissociation peak of GF. Additionally, the residual mass fraction for GO/GF is 12.6% at 800 °C after all the reactions end, which is smaller than the average of pure GO and GF (∼18.2% = (26.3% + 10.1%)/2), suggesting that more GO and GF have reacted to form gaseous products. Similarly, the amount of heat release integrated from the second exotherm (second ΔH in Figure 2b) in GO/GF (9.36 kJ/g) is larger than those in GO and GF (8.58 and 7.50 kJ/g, respectively), as shown in Figure 2c. In summary, the GO/GF mixture produces more gaseous products and releases more heat than the average values of two separated components, indicating a synergistic effect between GO and GF.

Similar to the TGA/DSC observations, the fast-heating T-jump time-of-flight mass spectrometry (TOFMS) experiments also show a synergistic effect between GO and GF (Figure 2d). The T-jump experiments provide onset temperatures for both C_xO_y species (e.g., CO_2, CO, C, and O) and CF_x species. First, pure GO has an onset temperature for C_xO_y of 373 ± 50 °C. Most of the signal for C_xO_y comes from the thermal reaction/decomposition product of the GO sample, and a small portion of C and O ion signals are from the fragmentation of CO_2 and/or CO; second, pure GF has only one onset temperature around 717 ± 50 °C, where mainly CF_x species are released from the dissociation of GF, while a small amount of C_xO_y species are also detected resulting from the oxygen residue in the system. Finally, the mixture of GO/GF (50/50 wt %) has a similar onset temperature of 362 ± 50 °C for C_xO_y as GO, but the onset temperature for CF_x (622 ± 50 °C) is about 95 °C lower than that of GF. This behavior is very similar to the TGA/DSC onset temperatures (Figure 2a,b). As such, both TGA/DSC and T-jump experiments confirm that the presence of GO facilitates the dissociation of GF.

https://dx.doi.org/10.1021/acsami.9b20397
ACS Appl. Mater. Interfaces 2020, 12, 7451−7458

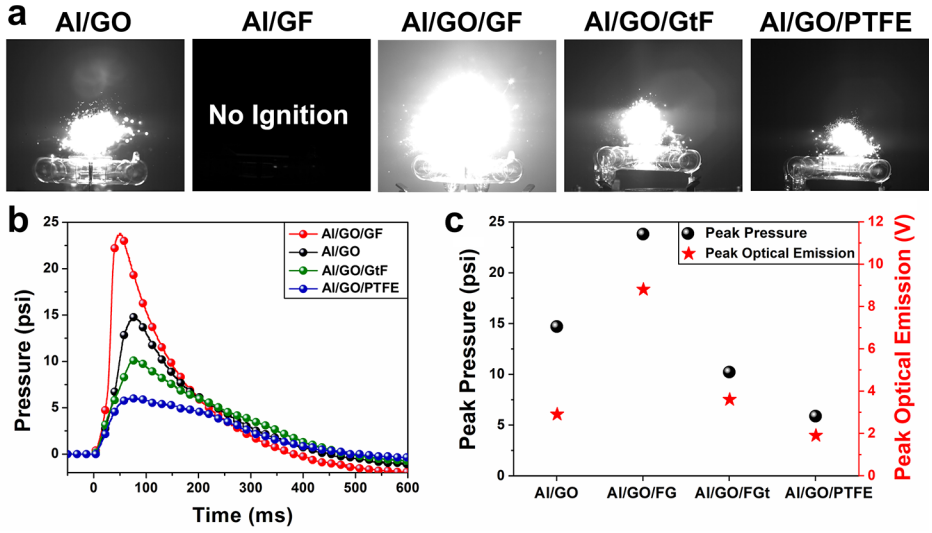

Figure 4. Comparison of the combustion performance of Al with different additives. (a) Snapshots of the burning of Al/GO (80/20 wt %), Al/GF (80/20 wt %), Al/GO/GF (80/10/10 wt %), Al/GO/GtF (80/10/10 wt %), and Al/GO/PTFE (80/10/10 wt %) composites at 40 ms after ignition by a Xe flash (power = 2.1 J/cm^2); (b) traces of the time-resolved pressure release evolution and (c) summary of the peak values of pressure release and optical emission of aforementioned Al composites (except Al/GF) ignited in a constant-volume reactor by a Xe flash (power = 2.1 J/cm^2).

3.2. RMD Simulations of Reaction Characteristics of GO, GF, and GO/GF Mixture in Air. To understand the interaction between GO and GF at the molecular level, we performed RMD simulations to investigate the chemical evolution of GO, GF, and GO/GF (mass ratio of 1:1) in O_2 at 2000 K. Figure 3a−c provide snapshots of the GO, GF, and GO/GF systems at t = 0 and 128 ps, respectively. At t = 128 ps, the GO/GF mixture appears to have fewer larger GO and GF sheets and more small-sized species than both pure GO and GF systems, indicating a faster dissociation of the GO and/or GF sheets. Figure 3d compares the dynamic change of the relative potential energy, which is the interatomic potential energy change with respect to the initial potential energy of the system. It shows that the relative potential energy of the GO/GF mixture drops much faster than that of pure GO and GF (Figure 3d), indicating a faster energy release. It should be noted that the larger fluctuations in the potential energy evolution of the GF or GO/GF system (compared with the pure GO system) may be attributed to additional reaction steps of F−O, F−C, and F−H interactions in RMD simulations. A closer inspection of the RMD simulation results reveals the chemical reaction pathways for GO and GF. Figure 3e illustrates a few key reactions. GF dissociates at high temperatures and generates CF_x radicals. CF_x radicals can be oxidized by gaseous O_2 to produce O and CF_xO_y radicals, a radical branching reaction. CF_x radicals can also be oxidized by O atoms on GO to form CF_xO_y radicals, which benefits both GF dissociation and GO disproportionation. Those RMD results suggest the molecular mechanisms on the experimentally observed synergistic interaction between GO and GF, which is caused by the accelerated radical generation and heat release.

3.3. Experiential Comparison of μ-Al Particle Combustion with GO, GF, GO/GF, and GO/Other Fluorinated Oxidizers as Additives. The above studies of GO and GF without Al demonstrate the chemical and thermal couplings between GO and GF due to radical reactions. Next, we investigate how those couplings affect μ-Al combustion by studying Al burning behavior to check the mechanism illustrated in Figure 1. We choose five control samples, all at 80 wt % of μ-Al particles with a diameter of 3.0−4.5 μm and 20 wt % of additives. The five additives are GO (20 wt %), GF (20 wt %), GO/GF (10/10 wt %), GO/GtF (10/10 wt %), and GO/PTFE (10/10 wt %). The two other fluorine-containing additives, GtF and PTFE, were included for comparison with GF. GtF is the bulk form of GF and has been reported as an effective additive for metal combustion as aforementioned.[26,27] PTFE is a widely studied oxidizer for Al combustion.[48] All the samples were pressed into pellets with a packing porosity of ∼83% and ignited by a Xe flash unit (AlienBees B1600). The experimental setup was illustrated in our previous work.[11] The flash pulse duration was about 5 ms and its integrated output power was about 2.1 J/cm^2.

Figures 4a and S1 show the high-speed video snapshots of the burning process of those five samples. First, all samples, except Al/GF, can be ignited by the Xe flash lamp, indicating that GO is critical for the optical initiation due to its strong light absorption property. GF is transparent and cannot absorb much energy from the Xe flash lamp. Second, the Al/GO/GF (80/10/10 wt %) sample shows the most violent burning among all five samples. This suggests the synergistic benefits of GO/GF and also shows that GF exhibits a stronger enhancing effect for Al/GO combustion than GtF and PTFE. The comparison between Al/GO/GF and Al/GO/GtF implies that the ultrathin fluorinated graphene is more effective than the bulk fluorinated graphite, probably due to the higher specific surface area, finer dispersion, and easier access to F of GF. However, the performance of Al/GO/GF is also better than that of Al/GO/PTFE, suggesting that GF is superior to the popular PTFE to improve the energetic performance of Al.

Next, we quantitatively compare the burning properties of these five samples by determining their dynamic pressure−time traces measured in a constant-volume glass vial. The details of the burning experimental setup can be found in our previous works.[11,49] Briefly, 20 mg of sample powders were packed into a pellet with a porosity of ∼83% in a 20 mL glass

https://dx.doi.org/10.1021/acsami.9b20397
ACS Appl. Mater. Interfaces 2020, 12, 7451−7458

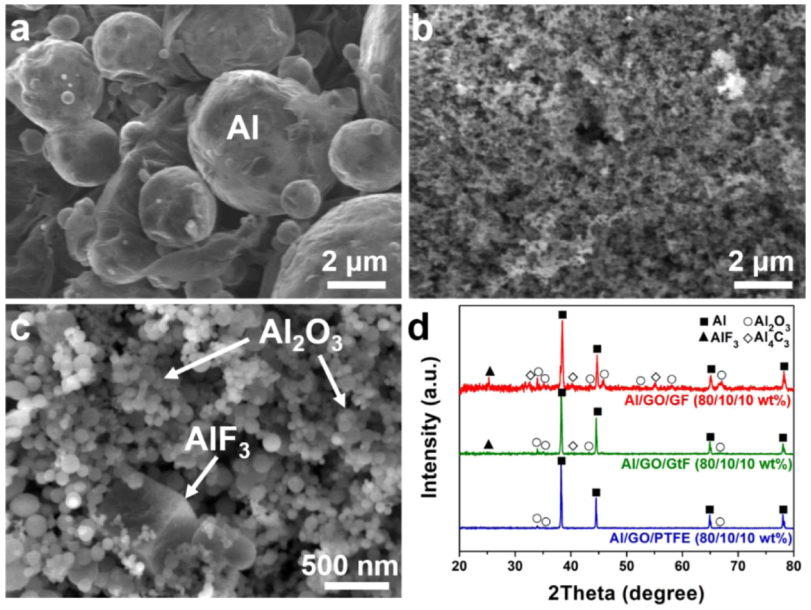

Figure 5. Characterization of the morphology and composition of the as-prepared sample and post-combustion products. SEM images of (a) the as-prepared Al/GO/GF (80/10/10 wt %), (b) its post-combustion products in the air, and (c) the enlarged image of (b); (d) XRD results of the post-combustion products in air of Al composites with GO and different fluorine-containing additives. The formation of Al_2O_3 nanoparticles and AlF_3 nanocubes is confirmed by combining SEM and XRD results.

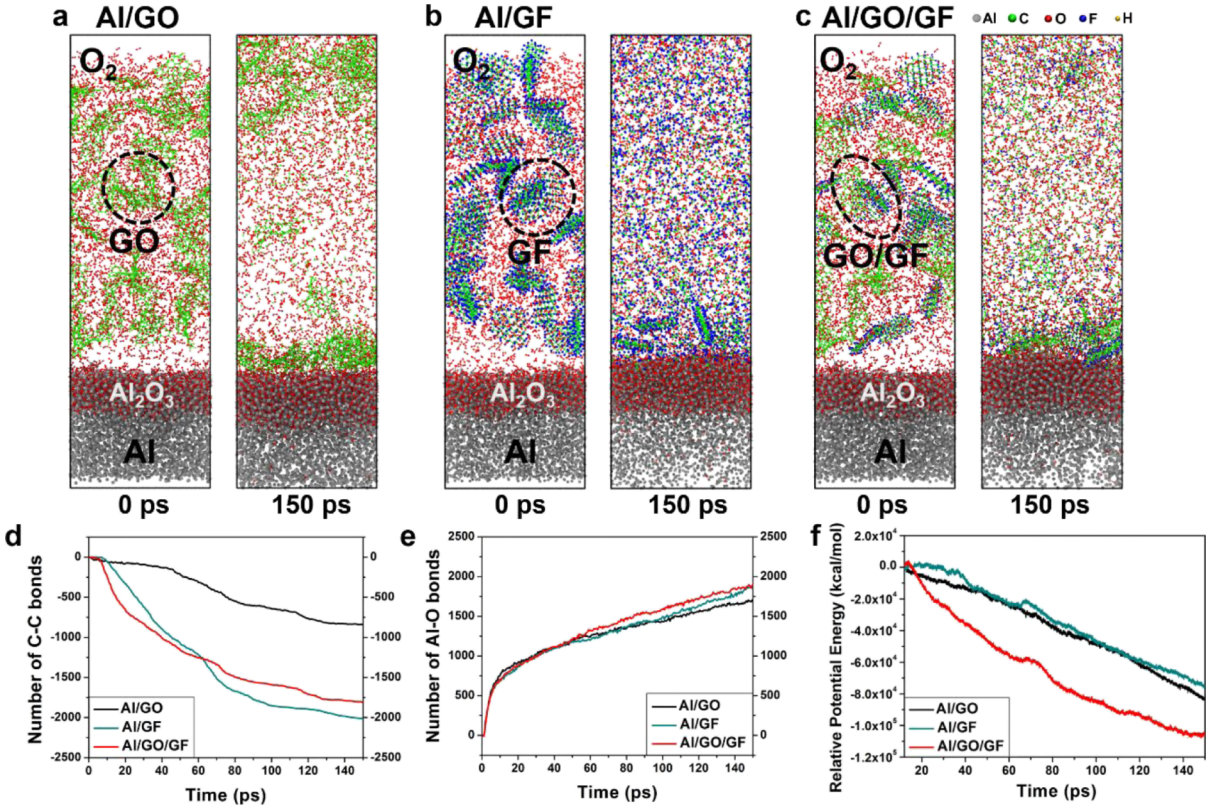

Figure 6. RMD simulation results reveal molecular-level thermal oxidation behaviors of Al/GO, Al/GF, and Al/GO/GF composites. Snapshots of RMD simulations of a pre-oxidized Al slab with (a) GO, (b) GF, and (c) GO/GF 1:1 mixture with O_2 at 2500 K at t = 0 and 150 ps (gray, Al atoms; green, C atoms; red, O atoms; blue, F atoms; yellow, H atoms); calculated number of (d) C−C bonds vs time and (e) Al−O bonds vs time; (f) the relative potential energy vs time. A lower relative potential energy indicates more heat release.

vial with ambient air inside. The vial was placed on top of the Xe flash unit, the samples were ignited at full power (2.1 J/cm^2), and the time-resolved pressure and optical emission of the vial were recorded by a pressure transducer (603B1, Kistler Inc.) and a photodiode (PDA36A, Thorlabs Inc.). Figure 4b shows the representative pressure−time traces of four control samples, except Al/GF, since Al/GF cannot be ignited. The peak pressures in Figure 4b and the peak optical intensity are

https://dx.doi.org/10.1021/acsami.9b20397
ACS Appl. Mater. Interfaces 2020, 12, 7451−7458

summarized in Figure 4c. The Al/GO/GF (80/10/10 wt %) mixture exhibits the highest peak pressure, pressure rise rate, and optical emission intensity, when compared with Al/GO, Al/GO/GtF, and Al/GO/PTFE samples. Even the Al/GO/GtF burns better than Al/GO/PTFE. Finally, the TGA/DSC results (Figure S2) of Al/GO (80/20 wt %) and Al/GO/GF (80/10/10 wt %) also demonstrate that Al/GO/GF has a higher specific heat release than Al/GO. The above results of pressure generation, optical emission, and heat release are consistent with the qualitative trend in the luminosity shown in Figures 4a and S1, indicating that the GO/GF is a more powerful additive than GO only for Al combustion.

3.4. Characterization of Al/GO/GF Post-Combustion Products. The post-combustion products of Al/GO/GF (from constant-volume pressure test) were further characterized to understand the combustion process. Figure 5a–c show the scanning electron microscopy (SEM) images of the as-prepared Al/GO/GF composites and corresponding post-combustion products. The as-prepared sample contains spherical Al particles with an average diameter of 3–4.5 μm, and the Al particles appear to be wrapped by GO and GF sheets. After flash ignition and combustion, the combustion products are porous and composed of mainly spherical nanoparticles (Figure 5b,c), which are supposed to be Al_2O_3. There are some sub-micron-sized cubes in the products (Figure 5c), which contains both Al and F according to the element mapping from energy-dispersive X-ray spectroscopy (EDXS), as shown in Figure S3. Additionally, X-ray diffraction (XRD) spectra show the crystalline phase compositions within the products (Figure 5d). The main products are Al_2O_3 and Al_4C_3 for all Al composites with GO and different fluorine-containing additives. The Al/GO/GF sample shows an obvious peak of AlF_3. The formation of AlF_3 cubes is confirmed by both SEM/EDXS and XRD, which was also observed by previous studies on Al reaction with fluoropolymers.[50,51] The formation of AlF_3 suggests that fluorine from GF reacts with Al and the fluorination of Al is one of the reasons for the enhanced performance of the Al/GO/GF sample.

3.5. RMD Simulations of μ-Al Oxidation with GO, GF, and GO/GF as Additives. To understand the effect of GO/GF interaction on μ-Al combustion at the molecular level, we conducted RMD simulations for three systems: Al/GO, Al/GF, and Al/GO/GF. Each system has a total number of 13,414 atoms, including a pre-oxidized Al slab and 2000 O_2 molecules. In addition, the Al/GO system contains 32 GO sheets; the Al/GF system contains 32 GF sheets; the Al/GO/GF system contains 16 GO sheets and 16 GF sheets. We exposed each system to 2500 K at t = 0 ps and let the system evolve until t = 150 ps. Figure 6a–c show snapshots of the Al/GO, Al/GF, and Al/GO/GF systems at t = 0 and 150 ps, respectively. At t = 150 ps, the Al/GO/GF system appears to have fewer larger GO and GF sheets than both Al/GO and Al/GF system, similar to the cases without Al (Figure 3a–c). The number of broken C–C bonds in Al/GO/GF (1818 at t = 150 ps) is also larger than the average value of those in Al/GO and Al/GF [(839 + 2013)/2 = 1426 at t = 150 ps] (Figure 6d), which implies that more GO disproportionation/oxidation and GF dissociation occurred in Al/GO/GF. The Al/GF system (Figure 6b) shows a higher degree of dissociation (e.g., more C–C bonds break) and Al oxidation (e.g., more Al–O bonds formation) than the Al/GO system (Figure 6e), but a similar energy release as the Al/GO composites (Figure 6f). These results imply that the CF_x and CF_xO_y species released/oxidized from GF facilitate Al oxidation/fluorination, but the dissociation and oxidation of GF are not as exothermic as the disproportionation and oxidation of GO, which is also consistent with the thermal analysis (Figure 2b,c). Interestingly, the relative potential energy in the Al/GO/GF mixture drops the fastest (Figure 6f), yielding the highest amount of energy release among the three systems. This suggests that the Al/GO/GF system reacts faster and releases more heat than Al/GO and Al/GF (Figures 6d–f and S4a–c for comparison).

These trends in the RMD simulations agree with our experimental observations. The energetic performance of Al particles is effectively enhanced with the mixture of the GO/GF sheets. Replacing the GO sheets with the GF sheets does not greatly improve the combustion of the Al particles. Only when both GO and GF are present, the ejected CF_x species could react with the GO sheets, in addition to O_2, to produce more CF_xO_y to react with Al, forming Al–O bonds faster (Figures 6e and S4).

4. CONCLUSIONS

In summary, we conducted both experimentally thermal analysis and RMD simulations to investigate the synergistic chemical and thermal interactions between GO and GF. The dissociation of GF generates CF_x species, which are readily oxidized by GO, forming CF_xO_y radicals. In other words, GO reacts with GF through radical reactions that facilitate the breakdown of GF and GO to release heat more rapidly. Since the interaction between GO and GF generates oxidative radicals and heat, this coupling was further used to accelerate the combustion (i.e., oxidation) process of μ-Al particles. We found that the Al/GO/GF composites exhibit improved energetic properties in terms of higher and faster pressure generation and stronger optical emission than Al/GO, Al/GF, and Al/GO/other fluorine-containing nanomaterials. These results demonstrate a new direction of utilizing chemical and thermal coupling reactions between ultrathin carbon materials to accelerate the combustion of Al and potentially oxidation reactions of other materials.

■ ASSOCIATED CONTENT

Supporting Information

The Supporting Information is available free of charge at https://pubs.acs.org/doi/10.1021/acsami.9b20397.

Time-resolved high-speed images showing the burning behaviors of Al composites; TGA/DSC results of Al/GO and Al/GO/GF composites; SEM/EDXS images of post-combustion products of Al/GO/GF composites in air; and evolutions of bond populations of Al/GO, Al/GF, and Al/GO/GF composites during RMD simulations (PDF)

■ AUTHOR INFORMATION

Corresponding Author

Xiaolin Zheng − *Department of Mechanical Engineering, Stanford University, Stanford, California 94305, United States;* orcid.org/0000-0002-8889-7873; Email: xlzheng@stanford.edu

https://dx.doi.org/10.1021/acsami.9b20397
ACS Appl. Mater. Interfaces 2020, 12, 7451–7458

Authors

Yue Jiang − *Department of Mechanical Engineering, Stanford University, Stanford, California 94305, United States;* orcid.org/0000-0002-6017-8551

Sili Deng − *Department of Mechanical Engineering, Stanford University, Stanford, California 94305, United States; Department of Mechanical Engineering, Massachusetts Institute of Technology, Cambridge, Massachusetts 02139, United States;* orcid.org/0000-0002-3421-7414

Sungwook Hong − *Collaboratory for Advanced Computing and Simulations, Department of Physics & Astronomy, Department of Computer Science, Department of Chemical Engineering & Materials Science, and Department of Biological Sciences, University of Southern California, Los Angeles, California 90089, United States; Department of Physics and Engineering, California State University, Bakersfield, Bakersfield, California 93311, United States;* orcid.org/0000-0003-3569-7701

Subodh Tiwari − *Collaboratory for Advanced Computing and Simulations, Department of Physics & Astronomy, Department of Computer Science, Department of Chemical Engineering & Materials Science, and Department of Biological Sciences, University of Southern California, Los Angeles, California 90089, United States;* orcid.org/0000-0002-5516-6900

Haihan Chen − *Department of Chemical and Environmental Engineering, University of California, Riverside, Riverside, California 92507, United States*

Ken-ichi Nomura − *Collaboratory for Advanced Computing and Simulations, Department of Physics & Astronomy, Department of Computer Science, Department of Chemical Engineering & Materials Science, and Department of Biological Sciences, University of Southern California, Los Angeles, California 90089, United States*

Rajiv K. Kalia − *Collaboratory for Advanced Computing and Simulations, Department of Physics & Astronomy, Department of Computer Science, Department of Chemical Engineering & Materials Science, and Department of Biological Sciences, University of Southern California, Los Angeles, California 90089, United States*

Aiichiro Nakano − *Collaboratory for Advanced Computing and Simulations, Department of Physics & Astronomy, Department of Computer Science, Department of Chemical Engineering & Materials Science, and Department of Biological Sciences, University of Southern California, Los Angeles, California 90089, United States;* orcid.org/0000-0003-3228-3896

Priya Vashishta − *Collaboratory for Advanced Computing and Simulations, Department of Physics & Astronomy, Department of Computer Science, Department of Chemical Engineering & Materials Science, and Department of Biological Sciences, University of Southern California, Los Angeles, California 90089, United States;* orcid.org/0000-0003-4683-429X

Michael R. Zachariah − *Department of Chemical and Environmental Engineering, University of California, Riverside, Riverside, California 92507, United States;* orcid.org/0000-0002-4115-3324

Complete contact information is available at: https://pubs.acs.org/10.1021/acsami.9b20397

Author Contributions

#Y.J., S.D. and S.H. contributed equally to this work.

Notes

The authors declare no competing financial interest.

■ ACKNOWLEDGMENTS

X.Z. acknowledges the support by the Office of Naval Research, under award number N00014-19-1-2085. The work at the University of Southern California was supported as part of the Computational Materials Sciences Program funded by the U.S. Department of Energy, Office of Science, Basic Energy Sciences, under award number DE-SC0014607. The simulations were performed at the Argonne Leadership Computing Facility under the DOE INCITE and Aurora Early Science programs and at the Center for High Performance Computing of the University of Southern California. M.R.Z. and H.C. gratefully acknowledge support from the Army Research Office.

■ REFERENCES

(1) Rossi, C.; Zhang, K.; Esteve, D.; Alphonse, P.; Tailhades, P.; Vahlas, C. Nanoenergetic Materials for MEMS: A Review. *J. Microelectromech. Syst.* **2007**, *16*, 919−931.

(2) Yetter, R. A.; Risha, G. A.; Son, S. F. Metal Particle Combustion and Nanotechnology. *Proc. Combust. Inst.* **2009**, *32*, 1819−1838.

(3) He, W.; Liu, P.-J.; He, G.-Q.; Gozin, M.; Yan, Q.-L. Highly Reactive Metastable Intermixed Composites (MICs): Preparation and Characterization. *Adv. Mater.* **2018**, *30*, 1706293.

(4) Wang, J.; Jiang, X.; Zhang, L.; Qiao, Z.; Gao, B.; Yang, G.; Huang, H. Design and Fabrication of Energetic Superlattice Like-PTFE/Al with Superior Performance and Application in Functional Micro-initiator. *Nano Energy* **2015**, *12*, 597−605.

(5) Yang, M.; Liu, J.; Li, S.; Zhang, S.; Wang, Y.; He, C. Ultrafast Synthesis of Graphene Nanosheets Encapsulated Si Nanoparticles via Deflagration of Energetic Materials for Lithium-Ion Batteries. *Nano Energy* **2019**, *65*, 104028.

(6) Comet, M.; Martin, C.; Schnell, F.; Spitzer, D. Nanothermites: A Short Review. Factsheet for Experimenters, Present and Future Challenges. *Propellants, Explos., Pyrotech.* **2019**, *44*, 18−36.

(7) Brooks, K. P.; Beckstead, M. W. Dynamics of Aluminum Combustion. *J. Propul. Power* **1995**, *11*, 769−780.

(8) Huang, Y.; Risha, G. A.; Yang, V.; Yetter, R. A. Effect of Particle Size on Combustion of Aluminum Particle Dust in Air. *Combust. Flame* **2009**, *156*, 5−13.

(9) Sundaram, D.; Yang, V.; Yetter, R. A. Metal-Based Nanoenergetic Materials: Synthesis, Properties, and Applications. *Prog. Energy Combust. Sci.* **2017**, *61*, 293−365.

(10) Dreizin, E. L. Metal-Based Reactive Nanomaterials. *Prog. Energy Combust. Sci.* **2009**, *35*, 141−167.

(11) Jiang, Y.; Deng, S.; Hong, S.; Zhao, J.; Huang, S.; Wu, C.-C.; Gottfried, J. L.; Nomura, K.-i.; Li, Y.; Tiwari, S.; Kalia, R. K.; Vashishta, P.; Nakano, A.; Zheng, X. Energetic Performance of Optically Activated Aluminum/Graphene Oxide Composites. *ACS Nano* **2018**, *12*, 11366−11375.

(12) Sabourin, J. L.; Dabbs, D. M.; Yetter, R. A.; Dryer, F. L.; Aksay, I. A. Functionalized Graphene Sheet Colloids for Enhanced Fuel/Propellant Combustion. *ACS Nano* **2009**, *3*, 3945−3954.

(13) Krishnan, D.; Kim, F.; Luo, J.; Cruz-Silva, R.; Cote, L. J.; Jang, H. D.; Huang, J. Energetic Graphene Oxide: Challenges and Opportunities. *Nano today* **2012**, *7*, 137−152.

(14) Thiruvengadathan, R.; Staley, C.; Geeson, J. M.; Chung, S.; Raymond, K. E.; Gangopadhyay, K.; Gangopadhyay, S. Enhanced Combustion Characteristics of Bismuth Trioxide-Aluminum Nanocomposites Prepared through Graphene Oxide Directed Self-Assembly. *Propellants, Explos., Pyrotech.* **2015**, *40*, 729−734.

(15) Gilje, S.; Dubin, S.; Badakhshan, A.; Farrar, J.; Danczyk, S. A.; Kaner, R. B. Photothermal Deoxygenation of Graphene Oxide for Patterning and Distributed Ignition Applications. *Adv. Mater.* **2010**, *22*, 419−423.

(16) Li, X.; Huang, B.; Li, R.; Zhang, H. p.; Qin, W.; Qiao, Z.; Liu, Y.; Yang, G. Laser-Ignited Relay-Domino-Like Reactions in Graphene

Oxide/CL-20 Films for High-Temperature Pulse Preparation of Bi-Layered Photothermal Membranes. *Small* **2019**, *15*, 1900338.
(17) Cote, L. J.; Cruz-Silva, R.; Huang, J. Flash Reduction and Patterning of Graphite Oxide and Its Polymer Composite. *J. Am. Chem. Soc.* **2009**, *131*, 11027−11032.
(18) Crouse, C. A. Fluorinated Polymers as Oxidizers for Energetic Composites. *Advances in Fluorine-Containing Polymers*; American Chemical Society, 2012; Vol. *1106*, pp 127−140.
(19) Kappagantula, K. S.; Farley, C.; Pantoya, M. L.; Horn, J. Tuning Energetic Material Reactivity Using Surface Functionalization of Aluminum Fuels. *J. Phys. Chem. C* **2012**, *116*, 24469−24475.
(20) Huang, S.; Pan, M.; Deng, S.; Jiang, Y.; Zhao, J.; Levy-Wendt, B.; Tang, S. K. Y.; Zheng, X. Modified Micro-Emulsion Synthesis of Highly Dispersed Al/PVDF Composites with Enhanced Combustion Properties. *Adv. Eng. Mater.* **2019**, *21*, 1801330.
(21) McCollum, J.; Pantoya, M. L.; Iacono, S. T. Activating Aluminum Reactivity with Fluoropolymer Coatings for Improved Energetic Composite Combustion. *ACS Appl. Mater. Interfaces* **2015**, *7*, 18742−18749.
(22) Watson, K. W.; Pantoya, M. L.; Levitas, V. I. Fast Reactions with Nano- and Micrometer Aluminum: A Study on Oxidation versus Fluorination. *Combust. Flame* **2008**, *155*, 619−634.
(23) Kim, D. W.; Kim, K. T.; Min, T. S.; Kim, K. J.; Kim, S. H. Improved Energetic-Behaviors of Spontaneously Surface-Mediated Al Particles. *Sci. Rep.* **2017**, *7*, 4659.
(24) Row, S. L.; Groven, L. J. Smart Energetics: Sensitization of the Aluminum-Fluoropolymer Reactive System. *Adv. Eng. Mater.* **2018**, *20*, 1700409.
(25) Wang, H.; Shen, J.; Kline, D. J.; Eckman, N.; Agrawal, N. R.; Wu, T.; Wang, P.; Zachariah, M. R. Direct Writing of a 90 wt% Particle Loading Nanothermite. *Adv. Mater.* **2019**, *31*, 1806575.
(26) Koch, E.-C. Metal/fluorocarbon pyrolants: VI. Combustion Behaviour and Radiation Properties of Magnesium/Poly (Carbon Monofluoride) Pyrolant. *Propellants, Explos., Pyrotech.* **2005**, *30*, 209−215.
(27) Sippel, T. R.; Son, S. F.; Groven, L. J. Modifying Aluminum Reactivity with Poly(Carbon Monofluoride) via Mechanical Activation. *Propellants, Explos., Pyrotech.* **2013**, *38*, 321−326.
(28) Feng, W.; Long, P.; Feng, Y.; Li, Y. Two-Dimensional Fluorinated Graphene: Synthesis, Structures, Properties and Applications. *Adv. Sci.* **2016**, *3*, 1500413.
(29) Nair, R. R.; Ren, W.; Jalil, R.; Riaz, I.; Kravets, V. G.; Britnell, L.; Blake, P.; Schedin, F.; Mayorov, A. S.; Yuan, S.; Katsnelson, M. I.; Cheng, H.-M.; Strupinski, W.; Bulusheva, L. G.; Okotrub, A. V.; Grigorieva, I. V.; Grigorenko, A. N.; Novoselov, K. S.; Geim, A. K. Fluorographene: A Two-Dimensional Counterpart of Teflon. *Small* **2010**, *6*, 2877−2884.
(30) Liu, H. Y.; Hou, Z. F.; Hu, C. H.; Yang, Y.; Zhu, Z. Z. Electronic and Magnetic Properties of Fluorinated Graphene with Different Coverage of Fluorine. *J. Phys. Chem. C* **2012**, *116*, 18193−18201.
(31) Karlický, F.; Kumara Ramanatha Datta, K.; Otyepka, M.; Zbořil, R. Halogenated Graphenes: Rapidly Growing Family of Graphene Derivatives. *ACS Nano* **2013**, *7*, 6434−6464.
(32) Han, S. S.; Yu, T. H.; Merinov, B. V.; van Duin, A. C. T.; Yazami, R.; Goddard, W. A. Unraveling Structural Models of Graphite Fluorides by Density Functional Theory Calculations. *Chem. Mater.* **2010**, *22*, 2142−2154.
(33) Belenkov, M. E.; Chernov, V. M.; Belenkov, E. A. Structure of Fluorographene and Its Polymorphous Varieties. *J. Phys.: Conf. Ser.* **2018**, *1124*, 022010.
(34) Gong, P.; Wang, Z.; Wang, J.; Wang, H.; Li, Z.; Fan, Z.; Xu, Y.; Han, X.; Yang, S. One-Pot Sonochemical Preparation of Fluorographene and Selective Tuning of Its Fluorine Coverage. *J. Mater. Chem.* **2012**, *22*, 16950−16956.
(35) Robinson, J. T.; Burgess, J. S.; Junkermeier, C. E.; Badescu, S. C.; Reinecke, T. L.; Perkins, F. K.; Zalalutdniov, M. K.; Baldwin, J. W.; Culbertson, J. C.; Sheehan, P. E.; Snow, E. S. Properties of Fluorinated Graphene Films. *Nano Lett.* **2010**, *10*, 3001−3005.
(36) Ohkura, Y.; Rao, P. M.; Zheng, X. Flash Ignition of Al Nanoparticles: Mechanism and Applications. *Combust. Flame* **2011**, *158*, 2544−2548.
(37) Ohkura, Y.; Rao, P. M.; Sun Cho, I.; Zheng, X. Reducing Minimum Flash Ignition Energy of Al Microparticles by Addition of WO_3 Nanoparticles. *Appl. Phys. Lett.* **2013**, *102*, 043108.
(38) Yang, F.; Zhang, Y.; Yang, X.; Zhong, M.; Yi, Z.; Liu, X.; Kang, X.; Luo, J.; Li, J.; Wang, C.-Y.; Zhao, H.-B.; Fu, Z.-B.; Tang, Y.-J. Enhanced Photothermal Effect in Ultralow-Density Carbon Aerogels with Microporous Structures for Facile Optical Ignition Applications. *ACS Appl. Mater. Interfaces* **2019**, *11*, 7250−7260.
(39) Zhou, L.; Piekiel, N.; Chowdhury, S.; Zachariah, M. R. T-Jump/Time-of-Flight Mass Spectrometry for Time-Resolved Analysis of Energetic Materials. *Rapid Commun. Mass Spectrom.* **2009**, *23*, 194−202.
(40) van Duin, A. C. T.; Dasgupta, S.; Lorant, F.; Goddard, W. A. ReaxFF: A Reactive Force Field for Hydrocarbons. *J. Phys. Chem. A* **2001**, *105*, 9396−9409.
(41) Senftle, T. P.; Hong, S.; Islam, M. M.; Kylasa, S. B.; Zheng, Y.; Shin, Y. K.; Junkermeier, C.; Engel-Herbert, R.; Janik, M. J.; Aktulga, H. M. The ReaxFF Reactive Force-Field: Development, Applications and Future Directions. *npj Comput. Mater.* **2016**, *2*, 15011.
(42) Hong, S.; van Duin, A. C. T. Atomistic-Scale Analysis of Carbon Coating and Its Effect on the Oxidation of Aluminum Nanoparticles by ReaxFF-Molecular Dynamics Simulations. *J. Phys. Chem. C* **2016**, *120*, 9464−9474.
(43) Rahnamoun, A.; van Duin, A. C. T. Reactive Molecular Dynamics Simulation on the Disintegration of Kapton, POSS Polyimide, Amorphous Silica, and Teflon During Atomic Oxygen Impact Using the ReaxFF Reactive Force-Field Method. *J. Phys. Chem. A* **2014**, *118*, 2780−2787.
(44) Kim, S.-Y.; van Duin, A. C. T.; Kubicki, J. D. Molecular Dynamics Simulations of the Interactions between TiO_2 Nanoparticles and Water with Na^+ and Cl^-, Methanol, and Formic Acid Using a Reactive Force Field. *J. Mater. Res.* **2013**, *28*, 513−520.
(45) Nosé, S. A Unified Formulation of the Constant Temperature Molecular Dynamics Methods. *J. Chem. Phys.* **1984**, *81*, 511−519.
(46) Hoover, W. G. Canonical Dynamics: Equilibrium Phase-Space Distributions. *Phys. Rev. A: At., Mol., Opt. Phys.* **1985**, *31*, 1695.
(47) Wang, X.; Dai, Y.; Wang, W.; Ren, M.; Li, B.; Fan, C.; Liu, X. Fluorographene with High Fluorine/Carbon Ratio: A Nanofiller for Preparing Low-κ Polyimide Hybrid Films. *ACS Appl. Mater. Interfaces* **2014**, *6*, 16182−16188.
(48) Collins, E. S.; Skelton, B. R.; Pantoya, M. L.; Irin, F.; Green, M. J.; Daniels, M. A. Ignition Sensitivity and Electrical Conductivity of An Aluminum Fluoropolymer Reactive Material with Carbon Nanofillers. *Combust. Flame* **2015**, *162*, 1417−1421.
(49) Huang, S.; Deng, S.; Jiang, Y.; Zheng, X. Experimental Effective Metal Oxides to Enhance Boron Combustion. *Combust. Flame* **2019**, *205*, 278−285.
(50) Wang, H.; Kline, D. J.; Rehwoldt, M.; Wu, T.; Zhao, W.; Wang, X.; Zachariah, M. R. Architecture Can Significantly Alter the Energy Release Rate from Nanocomposite Energetics. *ACS Appl. Polym. Mater.* **2019**, *1*, 982−989.
(51) Kostoglou, N.; Emre Gunduz, I.; Isik, T.; Ortalan, V.; Constantinides, G.; Kontos, A. G.; Steriotis, T.; Ryzhkov, V.; Bousser, E.; Matthews, A.; Doumanidis, C.; Mitterer, C.; Rebholz, C. Novel Combustion Synthesis of Carbon Foam-Aluminum Fluoride Nanocomposite Materials. *Mater. Des.* **2018**, *144*, 222−228.

https://dx.doi.org/10.1021/acsami.9b20397
ACS Appl. Mater. Interfaces 2020, 12, 7451−7458